Journal of Nuclear and Radiochemical Sciences, Vol. 8, No. 2, pp. 79-84, 2007

TDPAC and Its Application to Chemistry

Y. Ohkubo,*[a] Y. Murakami,[b] W. Sato,[c] and A. Yokoyama[d]

[a]*Research Reactor Institute, Kyoto University, Kumatori, Osaka 590-0494, Japan*
[b]*Graduate School of Science, Kyoto University, Kyoto 606-8502, Japan*
[c]*Graduate School of Science, Osaka University, Toyonaka, Osaka 560-0043, Japan*
[d]*Graduate School of Natural Science and Technology, Kanazawa University, Kanazawa, Ishikawa 920-1192, Japan*

Received: October 25, 2006; In Final Form: December 26, 2006

Time-differential perturbed angular correlation (TDPAC) is a powerful tool in material science for measuring the local electromagnetic fields at probe nuclei through hyperfine interactions. We have been applying this technique with reactor-made radioactive nuclei to several different material systems. In this paper, following a brief description of the TDPAC technique, our recent results are reviewed.

1. Introduction

This paper aims to fulfill two objectives. The first one is to outline the theory and technique of the time-differential perturbed-angular-correlation (TDPAC) method, which is a nuclear spectroscopic technique for investigating local structures, electronic states, etc., in materials via hyperfine interactions. A detailed account of the perturbed-angular-correlation theory is given by Frauenfelder and Steffen.[1] The second is to give a brief account of TDPAC experiments using the Kyoto University research reactor (KUR). Our recent results are those on the ferroelectric phase transition of $LiTaO_3$,[2] local magnetic fields in the Mo layer of Mo/Fe multilayer,[3] hopping motion of Ce in graphite,[4] and hyperfine fields in a protein, mavicyanin.[5]

2. Outline of the TDPAC Theory

The two γ rays in a cascade process emitted from an excited nucleus exhibit the angular correlation between them, which depends primarily on nuclear properties such as the multipolarities of the γ rays and the spins of the relevant levels. The angular correlation $W(\theta)$ is expressed as follows; $W(\theta)\mathrm{d}\Omega$ is the relative probability that the second γ ray is emitted into the solid angle $\mathrm{d}\Omega$ at an angle θ with respect to the emission direction of the first γ ray.

$$W(\theta) = \sum_k A_k(1)A_k(2)\,P_k(\cos\theta), \tag{1}$$

where the summation index k takes non-negative even integers with the upper limit determined by the values of the multipolarities of the two γ rays and the spin of the intermediate nuclear level, and P_k is the k_{th}-order Legendre polynomial. $A_k(1)$ and $A_k(2)$ are quantities concerning the first and second γ transitions, respectively, determined only by the nuclear properties.

When a nucleus in its intermediate level interacts with an extranuclear field, the angular correlation is perturbed. The general expression for the perturbed angular correlation is as follows:

$$W(\vec{p}_1,\vec{p}_2,t) = \sum_{k_1k_2N_1N_2} A_{k_1}(1)A_{k_2}(2)G_{k_1k_2}^{N_1N_2}(t)[(2k_1+1)(2k_2+1)]^{-1/2}$$

$$\times Y_{k_1}^{N_1\,*}(\theta_1,\varphi_1)Y_{k_2}^{N_2}(\theta_2,\varphi_2), \tag{2}$$

where $\vec{p}_1$ and $\vec{p}_2$ are the momenta of the first and second γ rays, respectively, and θ_i and φ_i (i = 1, 2) in the spherical harmonics are their spherical coordinates. Like $A_k(1)$ and $A_k(2)$ in eq 1, $A_{k_1}(1)$ and $A_{k_2}(2)$ are quantities concerning the first and second γ transitions, respectively, determined only by the nuclear properties. The parameters k_i (i = 1, 2) are non-negative even integers and N_i are integers satisfying $-k_i \le N_i \le k_i$. The perturbation factor $G_{k_1k_2}^{N_1N_2}(t)$ contains information on the interaction of the nucleus in its intermediate state having spin I with extranuclear fields and is written as

$$G_{k_1k_2}^{N_1N_2}(t) = \sum_{m_am_b} (-1)^{2I+m_a+m_b}[(2k_1+1)(2k_2+1)]^{1/2}\begin{pmatrix} I & I & k_1 \\ m'_a & -m_a & N_1 \end{pmatrix}$$

$$\times \begin{pmatrix} I & I & k_2 \\ m'_b & -m_b & N_2 \end{pmatrix}\langle m_b|\Lambda(t)|m_a\rangle\langle m'_b|\Lambda(t)|m'_a\rangle^*, \tag{3}$$

where the eigenvalues such as m_a in the 3-j symbols are referred to an arbitrarily chosen z-axis. The quantity $\Lambda(t)$ reflects the interaction of the nucleus with extranuclear fields. In the case of static interactions, $\Lambda(t)$ is written as $\exp(-iH_{\mathrm{int}}t/\hbar)$, where H_{int} is the time-independent interaction Hamiltonian. If there is no effective extranuclear field, i.e., $\Lambda(t)$ = 1, $G_{k_1k_2}^{N_1N_2}(t)$ is equal to $\delta_{N_1N_2}\delta_{k_1k_2}$ and eq 2 is thus reduced to eq 1, as it should be. Using the eigenvector $|n\rangle$ of H_{int} with the eigenvalue E_n, eq 3 is rewritten as

$$G_{k_1k_2}^{N_1N_2}(t) = \sum_{m_am_b}\sum_{n,n'} (-1)^{2I+m_a+m_b}[(2k_1+1)(2k_2+1)]^{1/2}e^{-(i/\hbar)(E_n-E_{n'})t}$$

$$\times\langle n|m_b\rangle^*\langle n|m_a\rangle\langle n'|m'_b\rangle\langle n'|m'_a\rangle^*\begin{pmatrix} I & I & k_1 \\ m'_a & -m_a & N_1 \end{pmatrix}\begin{pmatrix} I & I & k_2 \\ m'_b & -m_b & N_2 \end{pmatrix}. \tag{4}$$

If the perturbing field is of axial symmetry and the z-axis is chosen parallel to the symmetry axis,

*Corresponding author. E-mail: ohkubo@rri.kyoto-u.ac.jp. FAX: +81-72-451-2625.

© 2007 The Japan Society of Nuclear and Radiochemical Sciences
Published on Web 10/19/2007

$$G^{NN}_{k_1k_2}(t) = \sum_m [(2k_1+1)(2k_2+1)]^{1/2} \times \begin{pmatrix} I & I & k_1 \\ m'-mN \end{pmatrix} \begin{pmatrix} I & I & k_2 \\ m'-mN \end{pmatrix} e^{-(i/\hbar)(E_m-E_{m'})t}. \quad (5)$$

When the sample is a powder source, i.e., an ensemble of randomly oriented microcrystals, the perturbation factor must be averaged over the Euler angles which transform the laboratory coordinate system to the coordinate system of each microcrystal. As a result, the perturbation factor does not depend on the parameters N_1 and N_2:

$$G_{kk}(t) = \sum_{N,m_a,m_b} \sum_{n,n'} (-1)^{2I+m_a+m_b} \begin{pmatrix} I & I & k \\ m'_a-m_aN \end{pmatrix} \begin{pmatrix} I & I & k \\ m'_b-m_bN \end{pmatrix} e^{-(i/\hbar)(E_n-E_{n'})t} \times \langle n|m_b\rangle^* \langle n|m_a\rangle \langle n'|m'_b\rangle \langle n'|m'_a\rangle^*. \quad (6)$$

The angular correlation $W(\vec{p}_1, \vec{p}_2, t)$ has the form

$$W(\vec{p}_1, \vec{p}_2, t) = W(\theta, t) = \sum_k A_k(1)A_k(2)G_{kk}(t)P_k(\cos\theta), \quad (7)$$

where θ is the angle between $\vec{p}_1$ and $\vec{p}_2$. Since in this form the differences from the expression for the unperturbed angular correlation, eq 1, are only the factors $G_{kk}(t)$, they are particularly called the attenuation factors. When each microcrystal is of axial symmetry, $G_{kk}(t)$ has the simpler form

$$G_{kk}(t) = \sum_{n,n'} \begin{pmatrix} I & I & k \\ n' & -n & n-n' \end{pmatrix}^2 e^{-(i/\hbar)(E_n-E_{n'})t}. \quad (8)$$

Note that the perturbed angular correlation is observable even for polycrystals.

Here, as a simple example we give the expression for the case where a uniform static magnetic field is applied perpendicular to the plane on which two γ detectors and a sample containing TDPAC nuclei are situated. The magnetic field ($\vec{B}$) is axially symmetric, and the relevant expression is eq 5 with $E_m = m\hbar\omega_L$ (z-axis is taken parallel to $\vec{B}$). Here, ω_L is the Larmor frequency, and using the nuclear g-factor and nuclear magneton μ_N, it is defined as $\omega_L = -g\mu_N B/\hbar$. The exponential factor depends on $N = m-m'$ and thus can be moved outside the summation symbol. Using the orthogonality relation of the 3j-symbols, the perturbation factor is written as

$$G^{NN}_{kk}(t) = \exp(-iN\omega_L t), \quad (9)$$

where $k_1 = k_2 = k$. Substituting eq 9 into eq 2 leads to the expression

$$W(\theta, t) = \sum_{k=0}^{k_{\max}} A_k(1)A_k(2)P_k[\cos(\theta-\omega_L t)], \quad (10)$$

taking $\theta_1 = \theta_2 = 90°$ and $\varphi_2 - \varphi_1 = \theta$. Coincidence counts $N(\theta, t)$ of the cascade γ rays are given by

$$N(\theta, t) = \exp(-t \ln 2/t_{1/2})W(\theta, t), \quad (11)$$

where $t_{1/2}$ is the half-life of the intermediate state of the probe nucleus. Assuming that the maximum value of k is 2, the ratio $R(t)$ obtained with the coincidence counts at $\theta = 180°$ and 90° becomes

$$R(t) = [N(180°,t) - N(90°,t)] / [N(180°,t) + N(90°,t)] \approx \frac{3}{4}A_2(1)A_2(2)\cos(2\omega_L t), \quad (12)$$

From the measurements of the angular correlation, ω_L can be obtained. Once ω_L is obtained and when either of the two quantities g or B is known, the other quantity can be derived. TDPAC technique gives the product of such two quantities. One is concerned with nuclear properties such as g-factor

TABLE 1: Characteristics of γ-γ cascades appropriate for TDPAC

Decay mode Parent → Probe Half-life	I^π	Mean life / ns	μ / nm	Q / b	γ_1 / keV	γ_2 / keV	A_{22}
^{99}Mo $\xrightarrow{\beta^-}_{2.7\ d}$ ^{99}Tc	$5/2^+$	5.2	+3.291		740	181	+0.10
^{99}Rh $\xrightarrow{EC}_{16\ d}$ ^{99}Ru	$3/2^+$	29.6	−0.284	+0.231	528 353	90 90	−0.19 −0.15
^{100}Pd $\xrightarrow{EC}_{3.6\ d}$ ^{100}Rh	2^+	309	+4.324		84	75	+0.17
^{111}Ag $\xrightarrow{\beta^-}_{7.5\ d}$ ^{111}Cd					96	245	−0.13
^{111m}Cd $\xrightarrow{IT}_{49\ min}$ ^{111}Cd	$5/2^+$	123	−0.7656	+0.77	151	245	+0.18
^{111}In $\xrightarrow{EC}_{2.8\ d}$ ^{111}Cd					171	245	−0.18
^{117}Cd $\xrightarrow{\beta^-}_{2.5\ h}$ ^{117}In	$3/2^+$	77.3	+0.938	(−)0.59	90	344	−0.36
^{140}La $\xrightarrow{\beta^-}_{1.7\ d}$ ^{140}Ce	4^+	5.0	+4.35	0.35	329	487	−0.13
^{181}Hf $\xrightarrow{\beta^-}_{42\ d}$ ^{181}Ta	$5/2^+$	15.6	+3.29	(+)2.35	133	482	−0.20

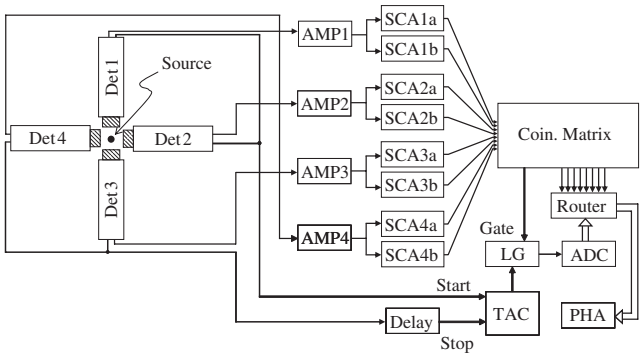

Figure 1. Block diagram of the TDPAC measurement system with four BaF_2 detectors.

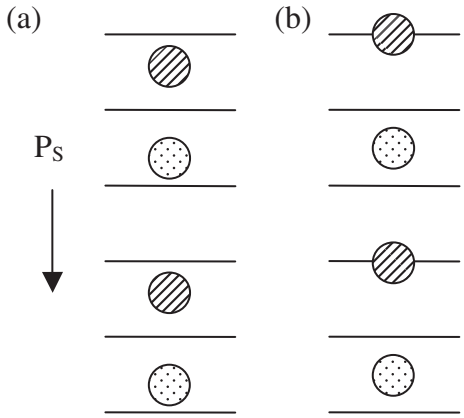

Figure 2. The (a) ferroelectric and (b) paraelectric structures of the $LiNbO_3$-$LiTaO_3$ system. The arrow indicates the direction of the spontaneous polarization (P_s) in the ferroelectric phase. Li is represented by the hatched, Nb (Ta) by the dotted circles. The horizontal lines stand for the oxygen planes.

which nuclear physicists are interested in and the other with material properties which chemists are interested in.

The expressions for the cases where the perturbing fields are static electric fields and dynamic ones are described in sec. 5 together with our recent TDPAC results.

3. TDPAC Probes

Conventional TDPAC probes are ^{99}Ru(←^{99}Rh), ^{100}Rh(←^{100}Pd), ^{111}Cd(←^{111}Ag), ^{111}Cd(←^{111m}Cd), ^{111}Cd(←^{111}In), ^{117}In(←^{117}Cd), ^{140}Ce(←^{140}La), and ^{181}Ta(←^{181}Hf). The relevant quantities for these probes are summarized in Table 1, together with those for ^{99}Tc(←^{99}Mo) used in our recent study on Mo/Fe multilayers. As seen from the half-life in Table 1, the time range during which interactions of nuclei with their surroundings are observed is the order of 10–1000 ns. ^{99}Ru and ^{100}Rh are especially useful for probing materials containing 4d transition elements. Likewise, ^{140}Ce is good for studying materials comprising rare-earth elements. ^{111}Cd can be produced from three different elements, Ag, Cd, and In. When these elements may occupy distinct sites in materials, corresponding ^{111}Cd-TDPAC measurements can bring more information than a single measurement using only one parent element. ^{111}Cd(←^{111m}Cd) and ^{117}In(←^{117}Cd) are an interesting pair. Both parent elements are the same, i.e., they occupy the same sites, but ^{111}Cd- and ^{117}In-TDPAC spectra may indicate that Cd and In behave differently (an example is given in sec. 5.1). Recently, ^{19}F arising from ^{19}O was used as a new TDPAC probe.[6]

4. TDPAC Measurement System

A measurement system can be constructed with standard fast-slow electronic modules and two γ detectors. However, it is often that four γ detectors are used and placed at right angles with each other on a plane. By doing this, 4 sets of $N(180°, t)$ and those of $N(90°, t)$ can be obtained at one measurement, so that a high measurement efficiency is gained. Moreover, this arrangement can avoid the unwanted effects owing to different detection efficiencies (which include the effect of different source-to-detector distances). For γ detection, scintillation detectors with high Z elements and good timing response are used. BaF_2 is such a scintillator. Figure 1 displays the block diagram of our TDPAC measurement system using four BaF_2 detectors.

5. Recent TDPAC Experiments Using the Kyoto University Research Reactor

5.1. Ferroelectric transitions in $LiNbO_3$ and $LiTaO_3$.[2]

Lithium niobate, $LiNbO_3$, and isostructural lithium tantalate, $LiTaO_3$, are ferroelectrics and are known as, for example, important non-linear optic materials. $LiNbO_3$ and $LiTaO_3$ adopt an ilmenite ($FeTiO_3$)-related structure (not the perovskite structure) because of the similar ionic sizes of Li^+ (76 pm), Nb^{5+} (64 pm), and Ta^{5+} (64 pm). These oxides undergo a structural phase transition (corresponding to a ferroelectric-to-paraelectric phase transition) at temperatures (T_C) of 1483 K and 938 K, respectively. The ferroelectric structure belongs to the $R3c$ space group. The atomic arrangement consists of oxygen octahedra sharing faces along the polar trigonal axis. When the spontaneous polarization direction is downward, the Nb (Ta) ion on this axis is displaced downward from the center of its octahedron [Figure 2(a)]. The next octahedron above contains a Li ion displaced upward from its center and the one more above has no metal ion inside it. The paraelectric structure belongs to the $R\bar{3}c$ space group. The Nb (Ta) ion is located at the center of its octahedron [Figure 2(b)]. The average Li position is on the upper-triangle oxygen base of the octahedron; the Li ion is disordered and occupies the previously empty octahedron half the time (dynamic disorder) or in half the unit cells (static disorder). In order to examine whether dynamic disorder takes place or static one does, TDPAC measurements using ^{111}Cd(←^{111m}Cd) and ^{117}In(←^{117}Cd) are effective. From a PIXE/channeling experiment, it is known that Cd (and also In) occupy the Li sites. If dynamic disorder is the right phenomenon, the temperature dependence of the quadrupole frequencies for ^{117}In and ^{111}Cd can be quite different, since the ionic radius of Cd^{2+} (95 pm) is so large that local dynamic disorder may be difficult to take place. On the other hand, the ionic radius of In^{3+} (80 pm) is comparable to that of Li^+ (76 pm), so that local dynamic disorder is not hampered. Since the bonding of In^{3+} with oxygen is stronger due to the higher charge, local dynamic disorder might take place at lower temperature than T_C, as is suggested by the fact that replacing a part of Li with In reduces T_C (e.g., T_C of $Li_{0.8}In_{0.067}TaO_3$ is 818 K,[7] 120 K reduction).

Typical TDPAC spectra of ^{117}In and ^{111}Cd in polycrystalline $LiTaO_3$ are shown in Figures 3(a) and 3(b), respectively. The ordinate $A_{22}G_{22}(t)$ was obtained as follows:

$$A_{22}G_{22}(t) = 2\,\frac{N(\pi,t) - N(\pi/2,t)}{N(\pi,t) + 2N(\pi/2,t)}\,. \qquad (13)$$

The quantity A_{22} is the same as $A_2(1)A_2(2)$ in eq 7. The pattern in each spectrum is modulated in a manner characteristic of a single electric quadrupole interaction in polycrystalline samples, depending on the spin value of the intermediate nuclear state. Since the Li site is of axial symmetry, the expected expressions of $G_{22}(t)$ for ^{117}In (I = 3/2) and ^{111}Cd (I = 5/2) are, respectively,

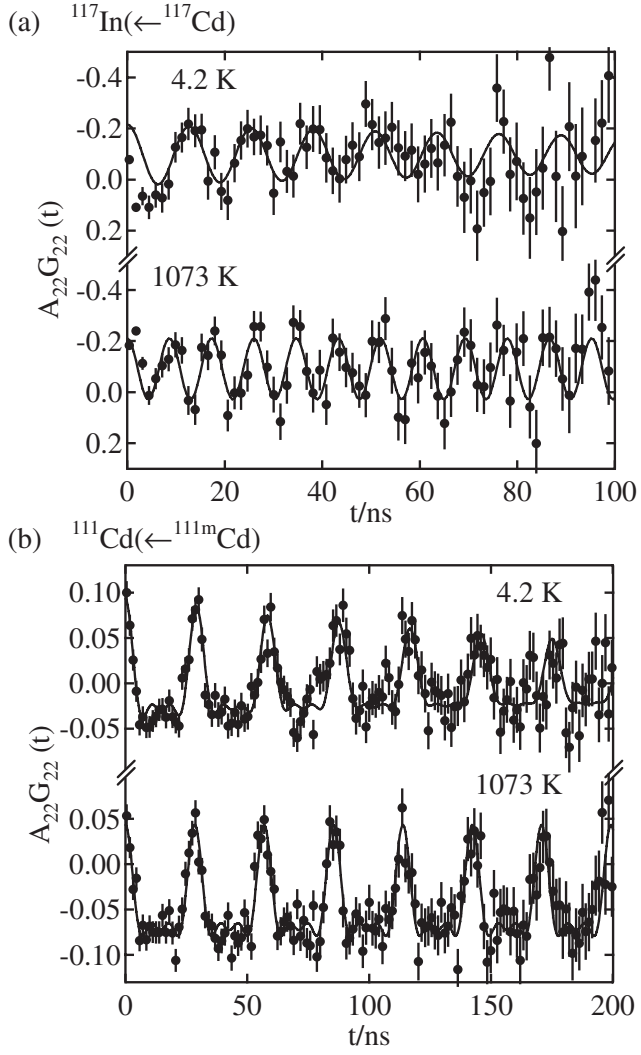

Figure 3. TDPAC spectra $A_{22}G_{22}(t)$ of (a) ^{117}In(←^{117}Cd) and of (b) ^{111}Cd(←^{111m}Cd) in $LiTaO_3$ at 4.2 and 1073 K with the solid curves representing the least-squares fits of eqs 14 and 15 in the text taking into account of ω_Q distributions.

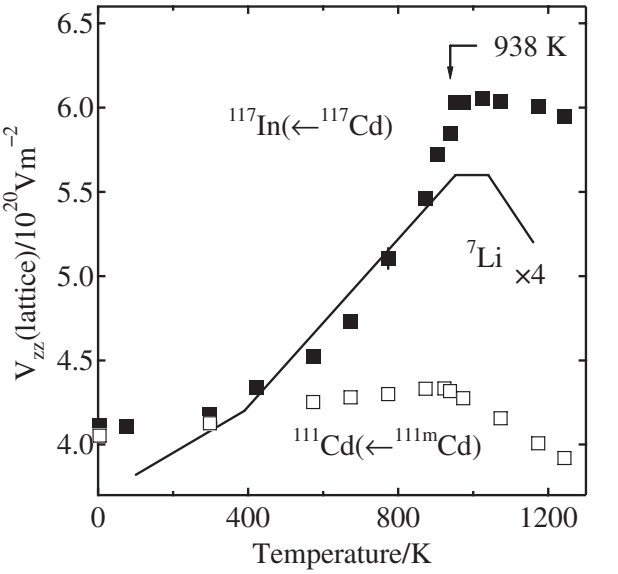

Figure 4. Temperature dependences of the lattice part of V_{zz} at ^{117}In (closed squares) and at ^{111}Cd (open squares) in $LiTaO_3$ with T_C = 938 K, together with that for ^{7}Li in $LiTaO_3$ (Reference 8) (solid line), which is multiplied by a factor of 4.

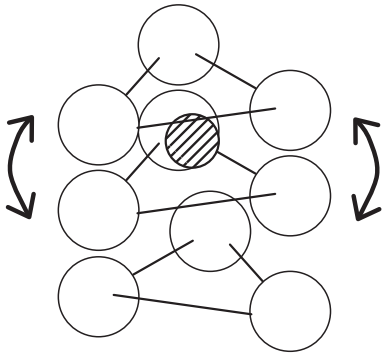

Figure 5. The local structure around a Li ion in the paraelectric phase of the $LiNbO_3$-$LiTaO_3$ system. Li is represented by the hatched, and O by the open circles. The two upper oxygen triangles represent a single one as being dynamically disordered.

$$G_{22}(t) = \frac{1}{5}[1 + 4\cos(6\omega_Q t)], \tag{14}$$

and

$$G_{22}(t) = \frac{1}{5}[1 + \frac{13}{7}\cos(6\omega_Q t) + \frac{10}{7}\cos(12\omega_Q t) + \frac{5}{7}\cos(18\omega_Q t)], \tag{15}$$

from eq 8 with $E_n = [3n^2 - I(I+1)]\hbar\omega_Q$, where ω_Q is the quadrupole frequency and is defined, using the nuclear electric quadrupole moment of the intermediate state Q and the largest component of the electric field gradient V_{zz} in the principal axis system, as $\hbar\omega_Q = eQV_{zz}/[4I(2I-1)]$. In the actual data analyses, $G_{22}(t)$ expressions without the assumption of axial symmetry were used and the results were consistent with the case of axial symmetry. Figure 4 displays the temperature dependences of V_{zz}(lattice) at ^{117}In and ^{111}Cd derived from dividing the obtained V_{zz} by a factor $(1 - \gamma_\infty)$ for each probe, where γ_∞ is the so-called Sternheimer antishielding factor. For comparison, also shown in Figure 4 is the temperature dependence of V_{zz}(lattice) at ^{7}Li obtained from ^{7}Li-NMR.[8]

As can be seen in Figure 4, the increase rate of V_{zz}(lattice) at ^{117}In is very large, comparable to the case of ^{7}Li, while in the case of ^{111}Cd it is small. In a certain temperature range above T_C, V_{zz}(lattice) at ^{117}In is constant, which is also true for the case of ^{7}Li, while in the case of ^{111}Cd there is no such constant region. The existence of the constant part means that the local system consisting of Li or In and oxygen ions is extremely stable, despite the high temperatures. These features fit very well the idea of dynamic disorder: Li or In of small ionic size comes closer to the center of three oxygen ions surrounding it together with other three oxygen ions, as the temperature increases; Above T_C, since there is enough space among the three oxygen ions due to thermal expansion, Li or In goes back and forth through this hole. This state is considered to be a sort of resonance state of high stability. On the contrary, Cd of large ionic size cannot move much toward the center of the three oxygen ions and thus cannot form a resonance state. Since the lowest temperature of the constant part of V_{zz}(lattice) at ^{117}In coincides with T_C, ions which actually disorder must be oxygen, not Li or In (Figure 5). Although we did not measure the TDPAC spectra for $LiNbO_3$ at temperatures near T_C because of high T_C, we expect that the similar dynamic disorder of oxygen ions takes place also in this material.

5.2. Local magnetic fields in the Mo layer of Mo/Fe multilayer.[3] Metallic multilayers consisting of ferromagnetic layers and nonmagnetic layers in alternate sequence display interesting magnetic phenomena. Oscillatory interlayer exchange coupling is an important example. As the nonmagnetic-layer thickness is varied, the coupling between two ferromagnetic layers sandwiching a nonmagnetic layer periodically

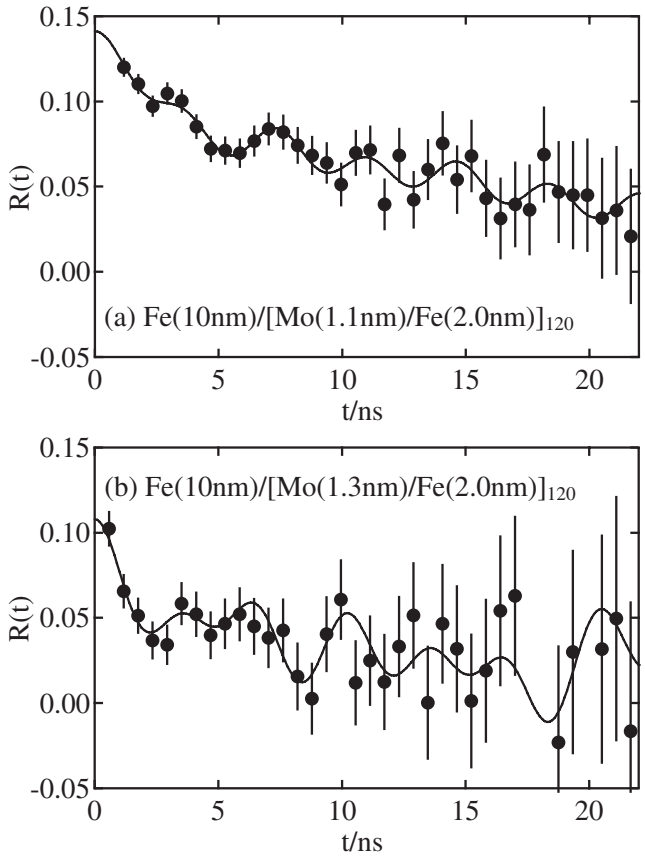

Figure 6. TDPAC spectra $R(t)$ at room temperature of ^{99}Tc(←^{99}Mo) in (a) Fe(10 nm)/[Mo(1.1 nm)/Fe(2.0 nm)]$_{120}$ and in (b) Fe(10 nm)/[Mo(1.3 nm)/Fe(2.0 nm)]$_{120}$ with the solid curves representing the least-squares fits of eq 16.

changes from being ferromagnetic to antiferromagenetic. Oscillatory interlayer exchange coupling is basically understood as due to the spin polarization of conduction electrons in the nonmagnetic layer, but local information about magnetic structure in the nonmagnetic layer is valuable.

Mo/Fe multilayer samples were prepared with the electron-beam evaporation technique: Fe(10 nm)/[Mo(d nm)/Fe(2.0 nm)]$_{120}$ (designed values of the Mo layer thickness d are 0.4, 0.7, 0.9, 1.1, and 1.3), the 10-nm Fe being a buffer layer, where the subscript indicates the number of the bilayers. These samples have bcc(110) texture and two neighboring Fe layers are ferromagnetically coupled with each other. The parent nuclei ^{99}Mo of the TDPAC probe ^{99}Tc were obtained by irradiating the samples with thermal neutrons. Figure 6 displays the room-temperature TDPAC spectra for Mo(d = 1.1 nm) and Mo(d = 1.3 nm). Assuming the perturbing fields are magnetic hyperfine fields, the TDPAC spectra were analyzed with the following expression:

$$R(t) = [N(\pi,t) - N(\pi/2,t)]/2^{-t/t_{1/2}}$$
$$= \frac{3}{4} A_{22} \sum_i P_i [a_{i0} + a_{i1}\cos(\omega_L^i t) + a_{i2}\cos(2\omega_L^i t)]. \quad (16)$$

Here, $t_{1/2}$ is the half-life of the intermediate state of the TDPAC probe, P_i is the fraction of the probe nuclei perturbed by the hyperfine magnetic fields B_i, and the values of a_{ij} (j = 0–2) depends on the orientation of the hyperfine field with respect to the detector plane, satisfying $\sum_j a_{ij} = 1$. ω_L^i is the Larmor frequency corresponding to B_i. Different from the case of the uniform magnetic field (see eq 1), here the term of $\cos(\omega_L t)$ appears in addition to $\cos(2\omega_L t)$, because in the present case the magnetic field is not axially symmetric. The solid curves in Figure 6 represent the results of the fit, which are summarized in Table 2. We consider that the different hyperfine fields roughly correspond to different Mo monolayers in a Mo layer, and that the monolayers for which the hyperfine fields are relatively large are those near the Mo/Fe interfaces. In Table 2, we note that especially the value of the hyperfine field near the Mo/Fe interface, B_1, for Mo(d = 1.3 nm) is larger than that for Mo(d = 1.1 nm).

TABLE 2: Hyperfine magnetic fields (B_i, i = 1–4) at ^{99}Tc in (A) Fe(10 nm)/[Mo(1.1 nm)/Fe(2.0 nm)]$_{120}$ and (B) Fe(10 nm)/[Mo(1.3 nm)/Fe(2.0 nm)]$_{120}$ at room temperature obtained with TDPAC

		i = 1	2	3	4
Sample A	B_i / T	13.6(3)	7.6(10)	5.5(6)	1.3(1)
	Fraction	0.2	0.2	0.2	0.4
Sample B	B_i / T	14.9(4)	9.6(4)	7.0(8)	1.4(3)
	Fraction	0.2	0.2	0.4	0.2

It is expected that the magnetization, M, in the Mo layer is a superposition of the magnetic profiles induced by the two interfaces [$M(x) = m(x) + m(d - x)$, where x is the distance from one of the interfaces]. For large nonmagnetic layer thicknesses (d ~ 10 monolayers), the magnetization caused by spin polarization from one side of the interface can be regarded as oscillating as[9]

$$m(x) = Cx^{-\alpha}\sin(2\pi x/\Lambda + \phi), \quad (17)$$

where Λ, ϕ, and α are, respectively, the oscillation period of interlayer coupling, a constant given by the electronic structure of the interlayer material, and the attenuation parameter. The thickness d affects coherence in the superposition of the spatially oscillating magnetizations arising from the two interfaces. Based on this model, the difference in the magnitude of the hyperfine field between the two Mo/Fe multilayer samples can be ascribed to the difference of the Mo layer thicknesses. For the present Mo(110)/Fe(110) multilayers, Λ is 1.2 nm and ϕ is 0 or π.[10] Assuming that the x dependence of B_1 is the same as that of $M(x)$, the value of the attenuation parameter α was derived from the dependence of B_1 on d to be about 2. This is in agreement with a theoretical value based on the RKKY mechanism for Cu/Fe and Ag/Fe.[11] We thus tentatively conclude that interlayer exchange coupling is due to RKKY interactions. Details of the experiments will be published elsewhere.

5.3. Hopping motion of Ce in graphite.[4] Related to TDPAC studies on Ce inside the cages of fullerenes, C_{82} and C_{80},[12,13] it is natural to extend the study to the cases of the other allotropes, graphite, and diamond. When Ce exists as Ce^{3+}, it has one 4f electron, and when Ce exists as Ce^{4+}, it has no unpaired electron. It is interesting to examine the state of Ce in these materials. Both samples containing ^{140}Ce were prepared by implanting 100-keV ^{140}Cs ions into highly oriented pyrolytic graphite (HOPG) and diamond samples using the isotope separator installed at KUR. The nucleus ^{140}Cs decays to ^{140}Ba, then ^{140}La, and finally ^{140}Ce.

The TDPAC spectra for diamond show that the relevant interaction is a weak static quadrupole one, indicating that Ce exists as Ce^{4+} and remains rest making chemical bonds with neighboring carbons.[13] However, the TDPAC spectra for HOPG are essentially of the exponential decay type, implying that Ce ions are hopping from one of its minimum energy sites to another. That Ce is moving in HOPG is similar to the case of fullerenes, although for fullerenes Ce is confined in the cage.

In order to examine the valence of Ce in graphite, a TDPAC spectrum was obtained under an external magnetic field of 0.84 T. If Ce exists as $Ce^{3+}$and has one 4f electron, the magnetic moment tends to be aligned with the direction of the applied magnetic field, so that the effective magnetic field at the Ce nucleus will be different from the external one, whereas if Ce exists as $Ce^{4+}$and has no unpaired electron, such a thing will not take place. The magnitude of a parameter of the so-called paramagnetic correction factor deduced from the TDPAC spectrum clearly indicates that Ce exists as Ce^{3+}. For both cases of HOPG and fullerenes, it was thus concluded that Ce exists as Ce^{3+}, and it is considered that this is related to the fact that both materials are electron donors.

5.4. Hyperfine fields in a protein, mavicyanin.[5] The structure around the metal site of mavicyanin, a relatively small protein molecule with a single copper site, has been investigated with ^{117}In- or ^{111}Cd-TDPAC. The main problem so far is that the parent nuclei, ^{117}Cd or ^{111m}Cd, are hard to locate at the copper site within a time comparable to their short half-lives (see Table 1). Preparing mavicyanin being also not an easy task, it is difficult to obtain TDPAC spectra with good statistics. We are planning to use ^{111}Ag as a parent nucleus to produce ^{111}Cd.

The preliminary results so far obtained are the electric field gradient (V_{zz}) values determined from the TDPAC spectra at pH 6.0, 7.5, and 8.0 for a mutant-type mavicyanin, Thr15Ala-Mav, as well as those for the wild-type. For both proteins there seems to be an abrupt change of V_{zz} between pH 6.0 and 7.5. What is interesting is that the V_{zz} values for the mutant-type mavicyanin are smaller than the corresponding values for the wild-type. This observation indicates that V_{zz} is sensitive to some structural change between the two types of mavicyanin, related to redox potential change found for them, although their UV-Vis spectra are identical with each other and thus do not provide information on the structural change.

Acknowledgement. This work was carried out in part under the Visiting Researcher's Program of the Research Reactor Institute, Kyoto University.

References

(1) H. Frauenfelder and R. M. Steffen, *Alpha-, Beta- and Gamma-ray Spectroscopy, Vol. 2*, Ed. K. Siegbahn, North-Holland, Amsterdam (1965), p 997.
(2) Y. Ohkubo, Y. Murakami, T. Saito, A. Yokoyama, S. Uehara, and Y. Kawase, Phys. Rev. B **65**, 052107 (2002); Y. Ohkubo, T. Saito, Y. Murakami, A. Yokoyama, and Y. Kawase, Mat. Trans. **43**, 1469 (2002).
(3) Y. Murakami, Y. Ohkubo, D. Fuse, Y. Sakamoto, Y. Hamada, T. Ono, S. Kitao, M. Seto, M. Tanigaki, T. Saito, S. Nasu, and Y. Kawase, Hyperfine Interact. **158**, 145 (2005).
(4) W. Sato, H. Ueno, A. Taniguchi, Y. Itsuki, Y. Kasamatsu, A. Shinohara, K. Asahi, K. Asai, and Y. Ohkubo, Phys. Rev. B **74**, 214302 (2006).
(5) A. Yokoyama, T. Hashimoto, H. Kikunaga, N. Kinoshita, Y. Murakami, K. Takamiya, and Y. Ohkubo, KURRI Prog. Rep. 2004, 60 (2005).
(6) W. Sato, H. Ueno, H. Watanabe, H. Miyoshi, A. Yoshimi, D. Kameda, T. Ito, K. Shimada, J. Kaihara, S. Suda, Y. Kobayashi, A. Shinohara, Y. Ohkubo, and K. Asahi (to be published).
(7) G.-T. Joo, J. Ravez, and P. Hagenmuller, Rev. Chim. minérale **22**, 18 (1985).
(8) D. Slotfeldt-Ellingsen and B. Pedersen, Phys. Status Solidi A **24**, 191 (1974).
(9) H. Luetkens, J. Korecki, E. Morenzoni, T. Prokscha, M. Birke, H. Glückler, R. Khasanov, H.-H. Klauss, T. Ślezak, A. Suter, E. M. Forgan, Ch. Niedermayer, and F. J. Litterst, Phys. Rev. Lett. **91**, 017204 (2003).
(10) D. D. Koelling, Phys. Rev. B **50**, 273 (1994).
(11) Q. Leng, V. Cros, R. Schäfer, A. Fuss, P. Grünberg, and W. Zinn, J. Magn. Magn. Mater. **126**, 367 (1993).
(12) W. Sato, K. Sueki, K. Kikuchi, K. Kobayashi, S. Suzuki, Y. Achiba, H. Nakahara, Y. Ohkubo, F. Ambe, and K. Asai, Phys. Rev. Lett. **80**, 133 (1998); W. Sato, K. Sueki, K. Kikuchi, S. Suzuki, Y. Achiba, H. Nakahara, Y. Ohkubo, K. Asai, and F. Ambe, Phys. Rev. B **58**, 10850 (1998).
(13) W. Sato, K. Sueki, Y. Achiba, H. Nakahara, Y. Ohkubo, and K. Asai, Phys. Rev. B **63**, 024405 (2001).